Journal of the Maharaja Sayajirao University of Baroda
ISSN: 0025-0422

ELECTRO-OPTICAL PROPERTIES OF CU-DOPED ZNS THIN FILM USED AS WINDOW LAYER IN SOLAR CELL

Arun S Garde Department of Physics, S P H Arts, Science and Commerce College Nampur 423204, India.

Jitendra A Borse Department of Physics, Late Pushpadevi Patil Arts & Science College Risod. 444506, India.

Abstract:
The simplified 2-electrode Electrochemical deposition method was carried out to prepare pure and Cu doped ZnS thin films on Fluorine doped tin oxide (FTO) glass and stainless steel substrate using an aqueous solution of 0.1M Zinc sulfate (ZnSO4), 0.1M Sodium thiosulphate (Na2S2O3). The 0.1M copper sulfate (CuSO4) was used as a dopant. The Cyclic voltammetry method was used to investigate the deposing potential of Zn, S, and Cu ions. The Cu-doping in ZnS thin film was achieved by adding different amounts of 0.1M CuSO4 solution in the main electrolyte bath. The XRD pattern of all film samples have seen a Zincblende cubic structure. The lattice constant and crystallite size decreases by increasing Cu in ZnS thin film. The Field Emission Scanning electron microscopy (FE-SEM) micrograph images showed some samples are composed of big grains with 135-375 nm dimension embedded in the matrix of nanoflakes. The average thickness of the nanoflakes was found to be 65.37 to 219.50 nm when copper doping was increased by 0-2% and decreased to 219.50-102.78 nm after increasing from 2-3%. The UV-Visible spectroscopy confirmed the energy band gap of Cu-doped ZnS thin film varied from 3.97- 2.11 eV. The electrical resistivity of ZnS thin film decreases with increasing Cu-doping. The hall coefficient values of the film samples showed the all deposited films are n-type electrical conductivity.
Keywords: Electrochemical deposition, Cu-doped ZnS thin film, Optical properties, electrical properties.

1. Introduction:

Zinc sulfide is an important society II-VI chalcogenide semiconductor material with a wide energy band gap which has application in solar cell, light-emitting diode, and photocatalysis [1]. The band gap of ZnS is about 3.95 eV. The optical band gap of ZnS makes it a potential material to replace CdS in heterojunction of CdS/CdTe solar cell [1]. The zinc sulfide is used as a window layer due to its suitable band gap. It allowed and delivered high- energy photons to absorbing material which improves the short circuit current in a solar cell. ZnS can be deposited by various techniques such as electrochemical deposition [2, 3], chemical bath deposition [4,], Chemical vapor deposition [5], physical vapor deposition, sputtering [6], atomic layer epitaxy, and SILAR method [7]. ZnS can be an n-type or p-type semiconductor in electrical conduction depending on the composition of Zn and S ions. The electrical conduction is important to the fabrication of solar cells [8]. The electrical conduction can be varied by various dopants [8]. The n-type ZnS as a window layer in ZnS/CdTe solar cell gives 12% efficiency [9]. The n-type or p-type electrical conductivity of ZnS can be achieved by varying the Zn/S ratio or suitable doping. The ZnS thin films with various dopants have been grown by many researchers by using different techniques. ZnS has a refractive index of 2.40. ZnS can be used as a reflector in optics because of its high reflective index [10]. ZnS can be used to manufacturing light-emitting diodes because of its wide energy bandgap [10]. The optical property of chalcogenide semiconductors depends on the size of their nanoparticles due to quantum confinement effect [11]. ZnS has two allotropic structures one is cubic sphalerite and another is wurtzite hexagonal structure [12]. Doping is the one method to tailor the energy bandgap. It influences optical, structural, and electrical properties. The transition metals such as Cu^{2+}, Ag^{2+}, Mn^{2+}, and Pb^{2+} can be dope in ZnS to achieve tunability of energy band gap [13]. It has been investigated by various techniques to reveal the effect of doping on the energy bandgap. The electro-optical properties of n-type ZnS thin films were analyzed by various atomic percentages of Cu-doped in ZnS material [14]. In this paper, the electrical parameters such as resistivity, mobility, hall coefficient, and carrier concentration have been investigated of Cu-doped ZnS thin films.

2. Experimental Details

2.1 Film Preparation

The Pure and Cu-doped ZnS thin film deposition was carried out by using a 2-electrode electrodeposition method consisting of stainless steel/FTO glass as working electrode, high purity graphite as counter electrode immersed in an electrolyte which is made up of pure distilled water. The aqueous electrolyte bath containing 0.1M $ZnSO_4$ (AR grade), 0.1M $Na_2S_2O_3$ (AR grade), and 0.1M $CuSO_4$ (AR Grade) were used as precursors for Zn, S, and Cu ions respectively [15]. 0.1M Triethanolamine was added to the electrolyte as a complexing agent [16]. The main electrolyte bath of 100 ml prepared by a mixed solution of 0.1M $ZnSO_4$ and 0.1M $Na_2S_2O_3$. The adding different amounts such as 1%, 2% and 3% correspond to 1 ml, 2 ml, and 3 ml of 0.1 M $CuSO_4$ as Cu-dopant added in the main electrolyte bath. The stainless steel (316 L) and FTO glass substrates are used for deposition. The stainless steel substrates were cleaned with double distilled water. The growth of ZnS and Cu was estimated by the cyclic voltammetry technique.

Figure.1 shows a 2-electrode simple electrochemical deposition setup.

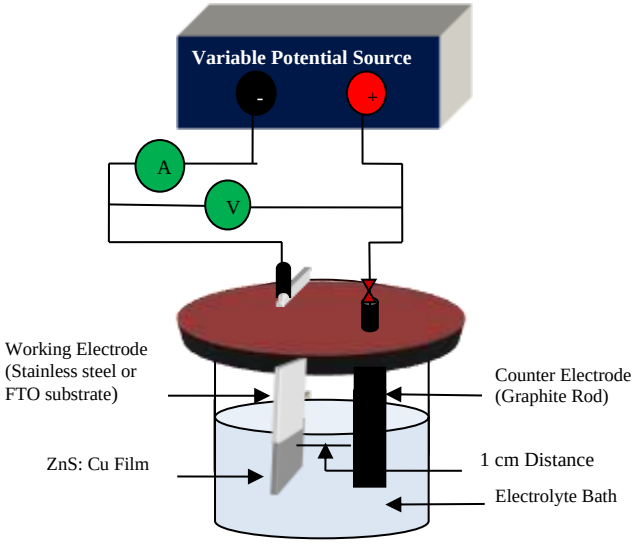

Fig.1. Schematic diagram of 2-electrode electrochemical deposition set up

The material is grown at fixed voltage by the electrochemical deposition method. 0.1M $CuSO_4$ of 1-3% of total electrolyte bath volume was added in the main electrolyte bath to achieve Cu-doping level in ZnS film. The deposition parameters are shown in **Table.1**. The resulting Pure and Cu-doped ZnS thin film samples were investigated by using X-ray diffraction (XRD), Field emission scanning electron microscope (FESEM), UV-visible spectrophotometer, and Hall Effect measuring system by Vander Pauw method for structural, surface morphology, optical properties, and electrical behavior respectively.

Table.1: Parameters of electrodeposition method for preparation of Cu-doped ZnS thin film

Sr. No.	Parameter	Value
1	Total quantity of electrolyte bath	100 ml
2	Bath composition	0.1 M $ZnSO_4$, 0.1 M $Na_2S_2O_3$, 0.1 M $CuSO_4$ & 0.1 M Triethanolamine (TEA)
3	Potential range applied	– 0.45 V to -1.0 V /Ag/AgCl (3-electrode set up) 1720 mv (2-electrode set up)
4	Deposition temperature	27^0C
5	pH	3.5
6	Substrate	Stainless steel, FTO glass

2.2 Film characterization

The X-ray diffraction pattern and identification of phase were obtained by X-ray diffractometer with Cu-Kα excitation wavelength of 1.54056 A^0. The average crystallite size was estimated by using Debye-Scherer's formula [17]. The optical bandgap of Pure and Cu-doped ZnS films were estimated by absorption spectra of films deposited on FTO glass and were measured using Carry 100 UV-Visible spectrophotometer in the range 100-800 nm [18]. The surface morphology of the film was observed using a field emission scanning electron microscope of model JEOL JSM-7600F. The resistivity, mobility, carrier concentration, and hall coefficient of Pure and Cu-doped ZnS thin film have been investigated by the Hall Effect measuring system of Vander Pauw method of ECOPIA model [19].

3. Result and Discussion

3.1 Cyclic Voltammetry

Figure.2 shows cyclic voltammetry of 0.1 M $CuSO_4$ solution. During forwarding scanning of potential, the two anodic peaks are found A1 and A2. The complete oxidation of Cu takes place at two anodic peaks.

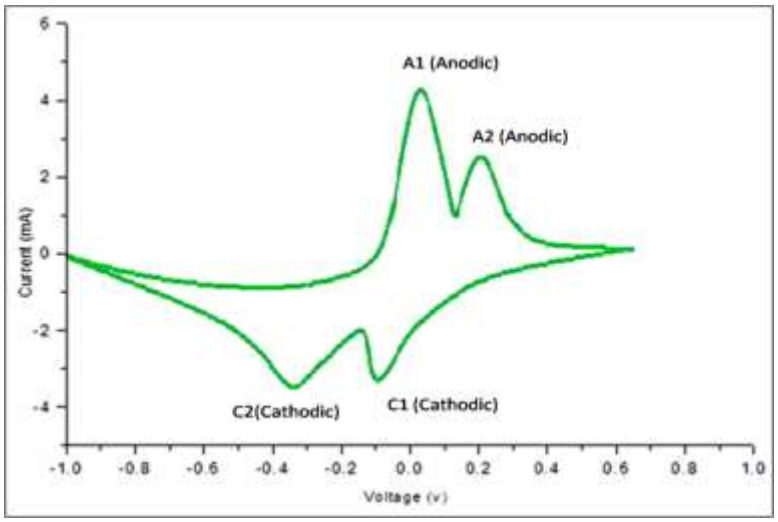

Fig.2. Cyclic Voltammograms of 0.1 M $CuSO_4$ solution

The oxidation reaction corresponds to peak A1 and A2 are given below.

A1: $Cu \longrightarrow Cu^{1+} + e$

A2: $Cu^{1+} \longrightarrow Cu^{2+} + e$

The anodic potential for oxidation of Cu was found at +0.2 V causes to the dissolution of Cu ion in an electrolyte bath. During reverse scanning, two cathodic potential peaks (C1 and C2) are found at -0.1 V and -0.35 V against Ag/AgCl (Reference Electrode) showed the reduction of copper ions. The reduction reactions correspond to peaks C1 and C2 are given below.

C1: $Cu^{2+} + e \longrightarrow Cu^{1}$

C2: $Cu^{1} + e \longrightarrow Cu$

The copper deposited at the cathodic potential in the range -0.1 V to -0.4 V against the Reference electrode (Ag/AgCl). The complete oxidation and reduction of copper ions are obtained in two successive steps. Figure.3 shows cyclic voltammetry for 0.1M $ZnSO_4$ and 0.1M $Na_2S_2O_3$ aqueous solution at scan speed 50 mv/sec to deposit ZnS. When the two solutions are mixed, the ZnS film growth voltage is estimated by the cyclic voltammetry technique. It indicates the variation of voltage with a current to estimate the appropriate deposing potential of ZnS thin film. The anodic peak was found in the range +0.5 V-+1.0 V at scan speed 50 mV/sec. The cathodic potential was reached at -0.75 V against Ag/AgCl (Reference Electrode). The appearance of a new reduction peak at -0.45 V due to the presence of Cu in the electrolyte.

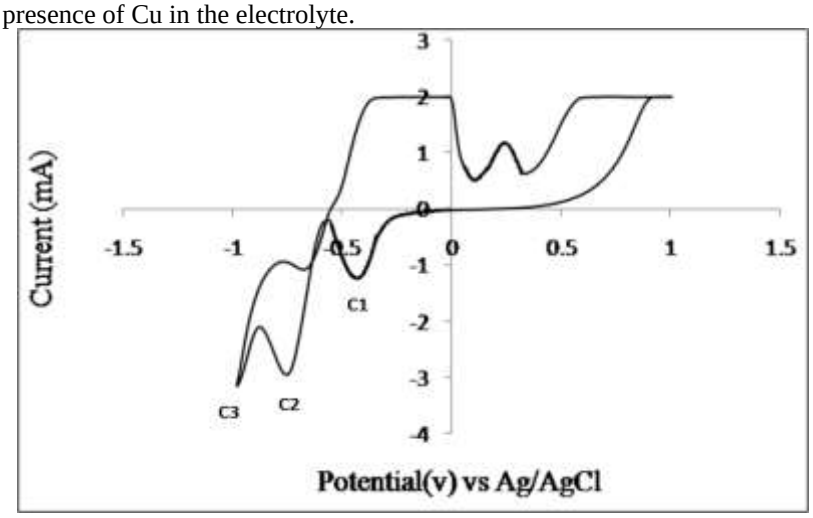

Fig.3. Cyclic Voltammograms of mixed bath of 0.1M $CuSO_4$, 0.1M $ZnSO_4$, and 0.1M $Na_2S_2O_3$ at scan rate 50mV/s.

It has been found that the deposing potential of ZnS with Cu content was observed at -0.75 V to -0.9 V. After investigating the electrochemical behavior of Zn, S, and Cu ions by using the cyclic voltammetry technique the deposition of Cu-doped ZnS thin film was carried out by a simple two-electrode electrodeposition technique. The area 2.25 cm^2 of substrate was selected for deposition of film.

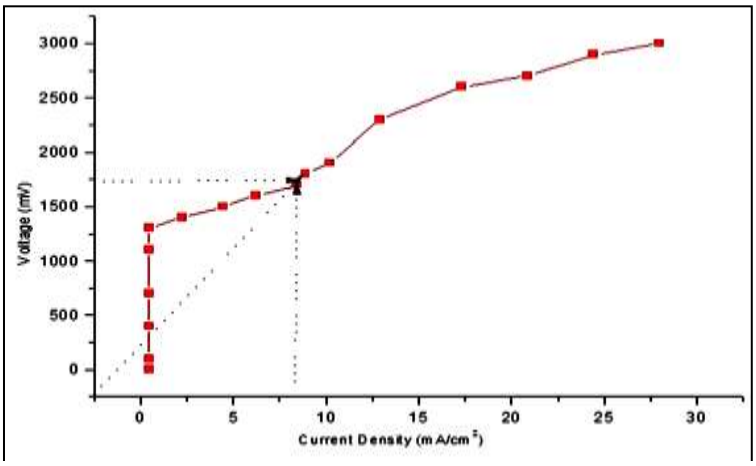

Fig.4. Polarization curve of mixed bath of 0.1M $ZnSO_4$ and 0.1M $Na_2S_2O_3$ for optimizing deposing potential in 2-electrode system

As per **Figure.4**, The potential 1720 mV was optimized corresponding current density 8.40 mA/cm^2 by plotting polarization curve of voltage versus current density for deposition of Cu-doped ZnS thin film in a 2-electrode system. The current density increases with increasing potential. The current density is current per unit deposited area of film.

3.2 Energy dispersive analysis by x-ray spectroscopy (EDAX)

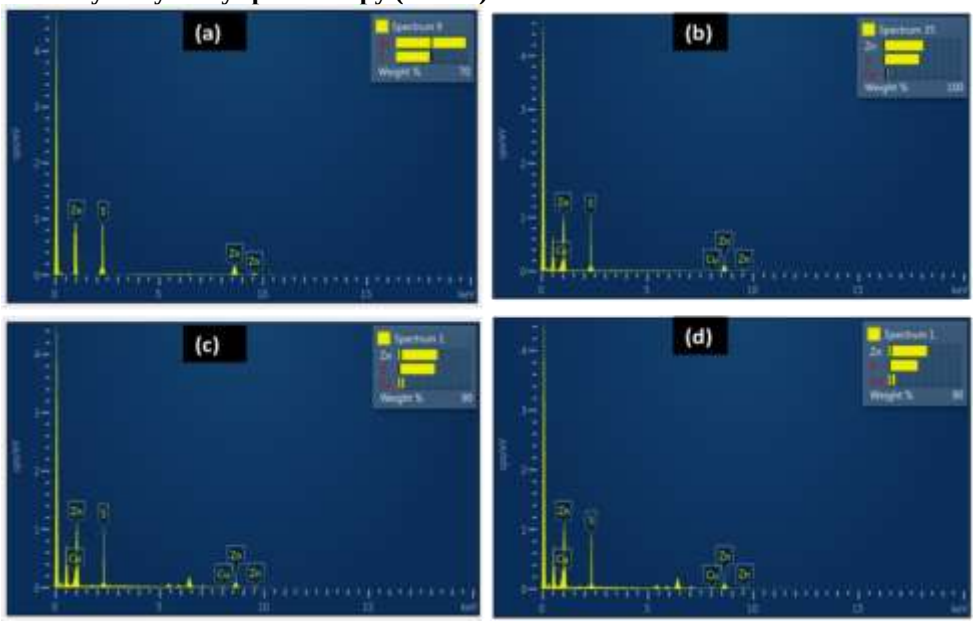

Fig.5. EDS spectrum of a) Pure ZnS b) ZnS: Cu (1%) c) ZnS: Cu (2%) d) ZnS: Cu (3%)

Figure.5 showed EDS spectrum of Un and Cu-doped ZnS thin film samples. As seen from spectrum the Cu- composition in deposited samples of undoped, ZnS: Cu (1%), ZnS: Cu (2%), and ZnS: Cu (3%) were observed about 0 at%, 0.6 at%, 6.32 at %, and 9.86 at% respectively. It has been confirmed the incorporation of increasing Cu ions in ZnS thin film without any impurity. The detailed composition of Zn, S, and Cu are listed in Table.2.

Table.2: Elemental composition of as prepared thin films samples

Samples	Zn (at %)	S (at %)	Cu (at %)	Total
a) Undoped ZnS	50.51	49.49	0	100
b) ZnS: Cu (1%)	50.00	49.40	0.60	100
c) ZnS: Cu (2%)	50.10	43.58	6.32	100
d) ZnS: Cu (3%)	50.14	40.00	9.86	100

3.3 X-ray Diffraction Analysis

Figure.6 shows the XRD pattern of Pure and Cu-doped ZnS thin films. After the XRD pattern is analyzed the peaks are observed at the orientation of plane (200), (220), (311), (222) and (400) are matched to the standard database (JCPDS data No.05-0566). It was confirmed the deposited ZnS film exhibit a Zincblende cubic structure without the founding secondary phase of CuS.

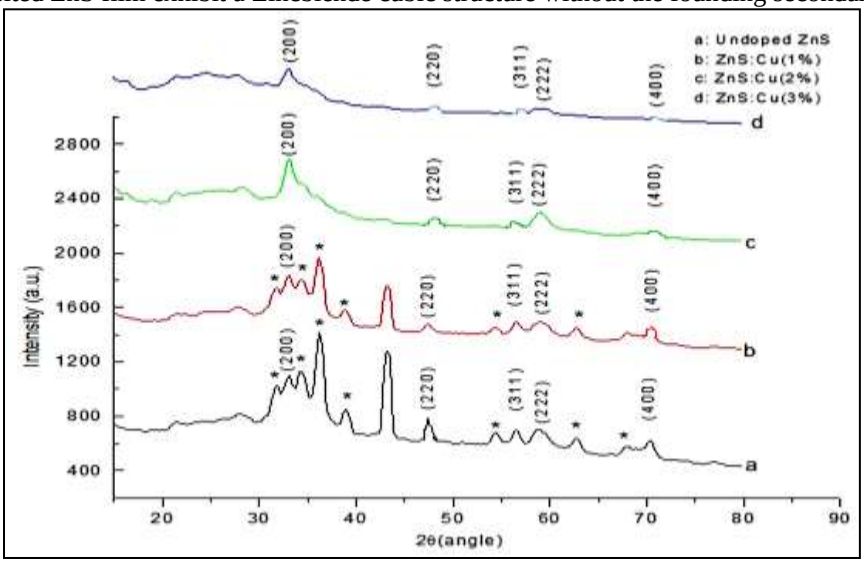

Fig. 6. XRD pattern of (a) Pure ZnS thin film (b) ZnS: Cu (1%) (c) ZnS: Cu (2%) (d) ZnS: Cu (3%)

The peaks denoted by * are matched to the standard database (JCPDS data No.33-0397) of stainless steel. It is confirmed * peaks indicate stainless steel substrate. As per the XRD pattern sample a of Pure ZnS exhibits high crystallinity than other Cu-doped ZnS samples [20, 21]. The intensity of peaks reduced with the incorporation of Cu ions in ZnS [22]. This is due to electronic density or point defect in lattice position and change in scattering factor. The crystallite size Pure and Cu-doped ZnS samples were estimated by using the Debye-Scherrer equation

$$D=\frac{0.9\lambda}{\beta cos\theta} \quad (1)$$

Where 'D' is the crystallite size, λ=1.5405 Å, 'β' is the full width at half maximum and 'θ' is the angle of diffraction. The crystallite size of Pure ZnS, ZnS: Cu (1%), ZnS: Cu (2%), and ZnS: Cu (3%) thin films for a plane (200) were estimated by using equation (1) about 34.46 nm, 24.41 nm, 20.72 nm, and 18.02 nm respectively. Consequently the crystallite size decreases and peak broadening and increases dislocation density and microstrain [23, 24]. The lattice constant was also affected by Cu-doping in ZnS and it was estimated by using the following equation.

$$a = d\sqrt{h^2 + k^2 + l^2} \quad (2)$$

Where d is interplanar spacing and (h k l) is the diffraction plane. The lattice constant for undoped ZnS thin film was found 5.452 A^0. Therefore, the lattice constant of ZnS: Cu (1%), ZnS: Cu (2%) and ZnS: Cu (3%) was found about 5.443 Å, 5.433 Å, and 5.424 Å respectively. The lattice constant is found to decreases with increasing Cu-doping in ZnS due to increasing microstrain and dislocation density upon Cu-doping. This is due to the ionic radius of Cu is less than Zn. So Cu ions are incorporated in the interstitial site of Zn. Hence lattice constant is affected by the ionic radius of the dopant. The dislocation density (δ) of deposited films was estimated by using the Williamson Smallman equation given below.

$$\delta = \frac{1}{D^2} \quad (3)$$

Where D is crystallite size. It is observed that the dislocation density increased by increasing Cu-doping in ZnS thin film. Subsequently, crystallite size decreases. The microstrain (ϵ) was estimated by using the following equation.

$$\epsilon = \frac{\beta}{4\tan\theta} \quad (4)$$

Where, β is full width at half maximum, the peak broadening with increasing Cu-doping. The broad peak indicates the lower intensity and large FWHM. The crystallite size is decreased by increasing Cu-doping this is due to lattice distortion or microstrain. Consequently, the sample ZnS: Cu (3%) shows a large lattice plane as compared to other samples. As per table.3 the microstrain is increased with increasing Cu-doping in ZnS nanostructure. The dislocation density and microstrain are observed maximum value in 3% Copper doped ZnS. The estimated values are listed in Table.3.

Table.3: Shows estimated values of average crystallite size, dislocation density and microstrain of a) undoped ZnS thin film b) ZnS:Cu (1%), c) ZnS:Cu (2%) and d) ZnS:Cu (3%) thin films.

Thin film Samples	2θ for plane (200)	FWHM	d-spacing	Lattice constant a(A^0)	Average Crystallite Size (nm)	Dislocation density(δ)x 10^{-3}(nm^{-2})	Microstrain (ϵ)x10^{-3}

Undoped ZnS	32.823	0.251	2.7264	5.452	34.46	0.8421	211.35
ZnS: Cu (1%)	32.883	0.357	2.7216	5.443	24.41	1.6782	276.40
ZnS: Cu (2%)	32.942	0.428	2.7168	5.433	20.72	2.3292	282.47
ZnS: Cu (3%)	33.02	0.501	2.7120	5.424	18.02	3.0795	290.87

3.4 UV-Visible Spectroscopy Analysis:

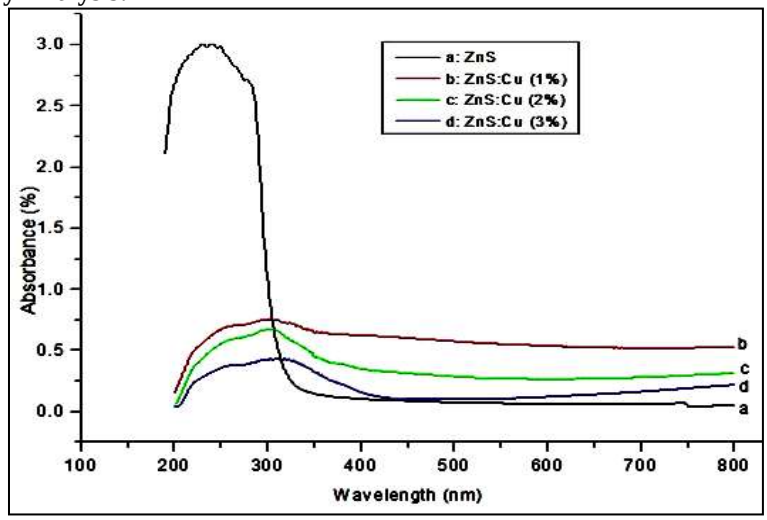

Fig.7. Optical Absorbance spectra of a) Pure ZnS b) ZnS: Cu (1%) c) ZnS: Cu (2%) d) ZnS: Cu (3%)

Figure.7 shows the UV-Visible absorption spectra of Pure and Cu-doped ZnS film thin films. The optical properties of films were investigated by a UV-Visible spectrophotometer with a wavelength range of 200-800 nm [25]. According to absorption spectra, the absorption edges are shifted to a higher wavelength 319 -412 nm with enhancing Cu-doping from 1-3% in ZnS thin film. This is a fundamental absorption edge. As a result, absorption increases with increasing Cu-doping percentage in ZnS. The energy band gap of Pure and Cu-doped ZnS thin film was estimated by tauc plotting of $(\alpha h\nu)^2$ versus hν by using the below equation.

$$\alpha h\nu = (h\nu - Eg)^n \qquad (5)$$

Where α is absorption coefficient, h is Planck's constant, ν is photon energy, E_g is optical bandgap and n is equal to ½ for direct band gap material. n is equal to 2 for allowed indirect, n is equal to 3/2 for non-radiative direct, n is equal to 3 for non-radiative indirect.

From **Figure 8**, the bandgap can be determined by the intercept of straight-line portion of $(\alpha h\nu)^2$ versus hν on hν axis [26]. It is observed that the energy band gap of Pure ZnS, ZnS: Cu (1%), ZnS: Cu (2%) and ZnS: Cu (3%) was found 3.97 eV, 3.07eV, 2.45eV, and 2.11 eV respectively. The estimated energy band gaps are listed in Table.4. As per Table.4 the bandgap energy decreases upon increasing Cu-doping due to increases in the specific surface area of ZnS nanostructure.

Table.4: Illustrate the estimated energy band gap values of Pure ZnS and Cu-doped ZnS thin films

Thin film Samples	Zn (at %)	S (at %)	Cu (at %)	Film thickness (nm)	Band gap energy (eV)
Undoped ZnS	50.51	49.49	0	954	3.97
ZnS: Cu (1%)	50.00	49.40	0.60	961	3.07
ZnS: Cu (2%)	50.10	43.58	6.32	960	2.45
ZnS: Cu (3%)	50.14	40.00	9.86	963	2.11

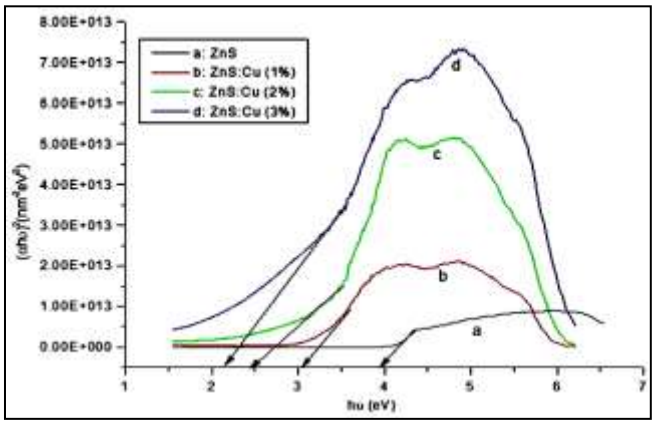

Fig.8. Energy Band Gap of a) Pure ZnS b) ZnS: Cu (1%) c) ZnS: Cu (2%) d) ZnS: Cu (3%)

Figure 8 shows the refractive index of Pure and Cu-doped ZnS thin film. The refractive index of Pure and Cu-doped ZnS thin films was estimated by using the following equation

$$n = \frac{1}{TS} + \sqrt{\frac{1}{Ts-1}} \qquad (6)$$

Where n is the refractive index, Ts is percent transmittance. The percent transmittance (Ts) was determined by using the following equation

$$Ts = 10^{(-A)}X100 \qquad (7)$$

Where A is the absorbance

From **Figure 9,** It has been observed that for all Pure and Cu-doped ZnS thin film samples, the refractive index (n) reduced with increasing wavelength. The Pure ZnS thin film has a high refractive index in the visible region. But the effects of Cu-doping the ZnS thin film are allowed to pass light of longer wavelength. The thin film samples Pure ZnS, ZnS: Cu (1%), ZnS: Cu (2%), and ZnS: Cu (3%) have greater transparency due to low refractive index for the wavelength 326 nm, 627 nm,718 nm, and 456 nm respectively. The thin film of ZnS: Cu (2%) has the highest transparency due to the low refractive index to wavelength 718 nm in the visible region. This allows employing this film layer as an optical window or buffer layer in the solar cell.

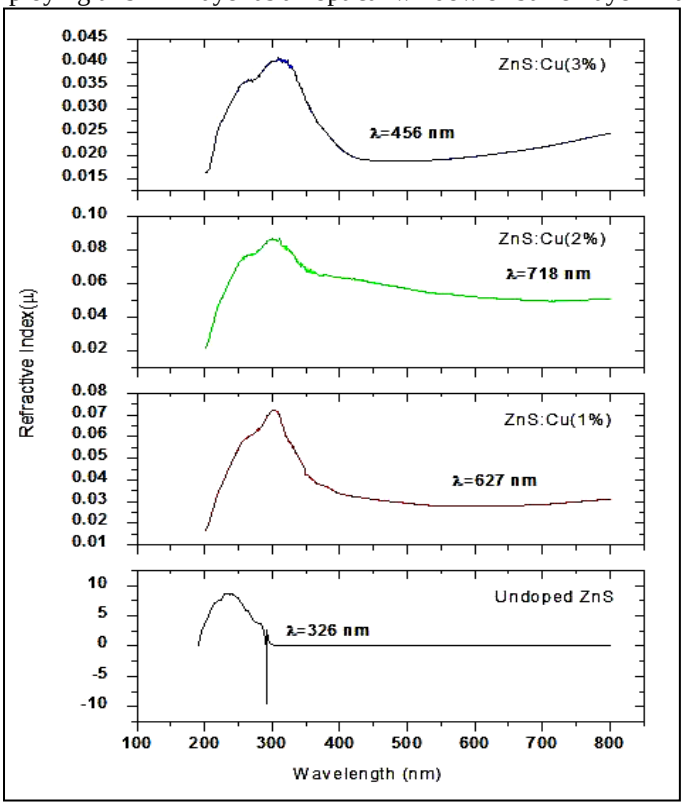

Fig.9. Illustrate the refractive index of Pure and Cu-doped ZnS thin film

3.5 Scanning Electron Microscopy (SEM) Analysis

Figure 10 illustrates the scanning electron micrograph (SEM) of ZnS films samples a, b, c, and d with different percentages of Cu content in ZnS thin films. As per FESEM micrograph images, all thin-film samples exhibit the same morphology. They showed some big grains with 135 to 375 nm dimensions composed in the matrix of nanoflakes of ZnS: Cu (2%) and ZnS: Cu (3%) thin films respectively. The average thickness of nanoflakes of sample Pure ZnS, ZnS: Cu (1%), ZnS: Cu (2%), and ZnS: Cu (3%) were observed about 65.37 nm, 88.74 nm, 219.50 nm, and 102.78 respectively. The sample 3% Copper doped ZnS shows hexagonal grain morphology. It is confirmed that the stress effect of Cu-doping on ZnS nanostructure [27].

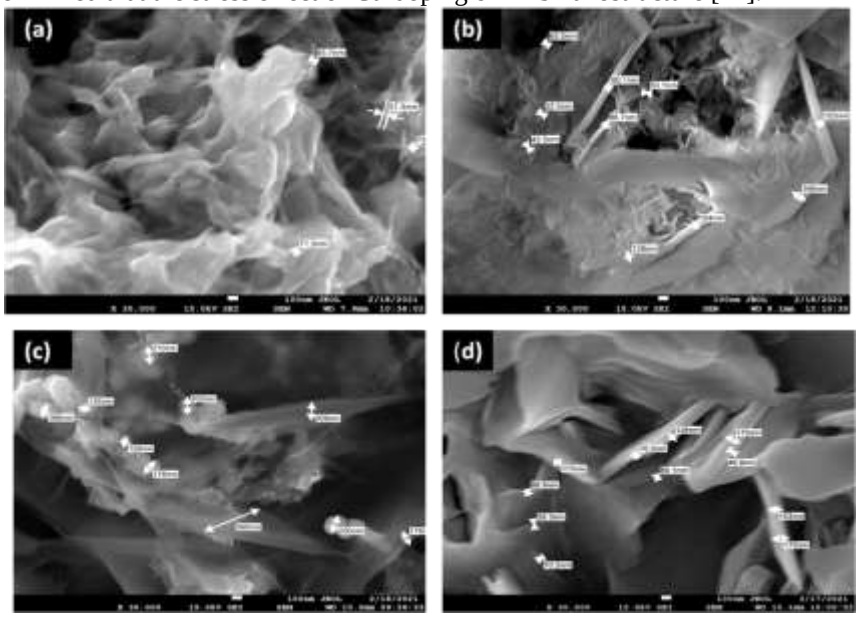

Fig.10 FESEM micrograph images of a) Pure ZnS thin film b) ZnS: Cu (1%) c) ZnS: Cu (2%) d) ZnS: Cu (3%)

3.6 Electrical properties by four probes Van Der Pauw method

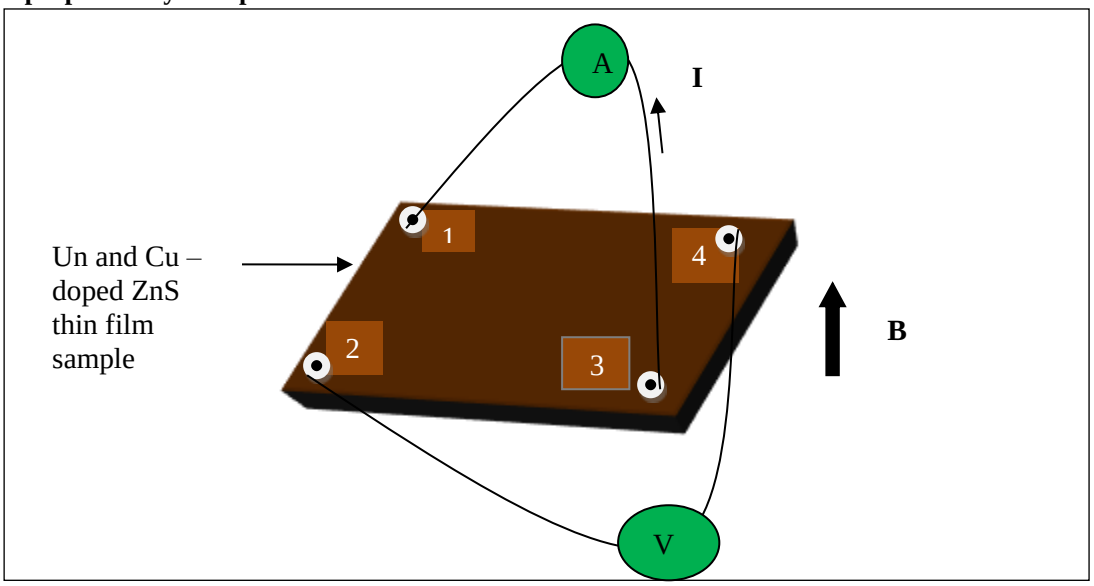

Fig.11 Schematic diagram of Vander Pauw method measuring system

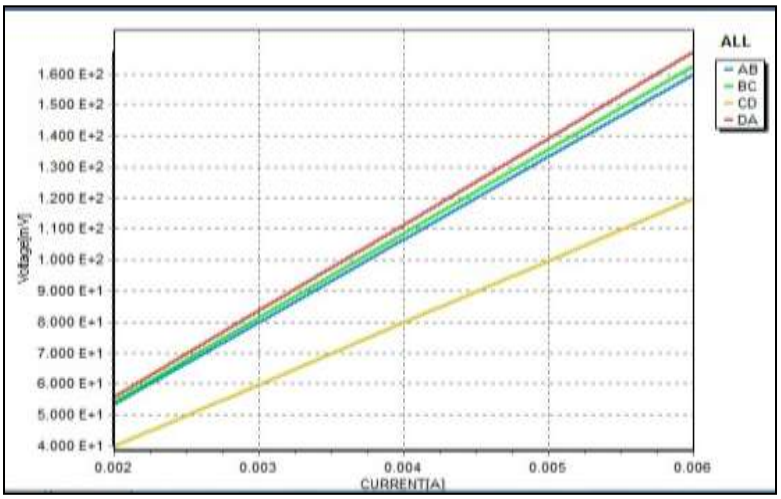

Fig.12 (a) Current- Voltage sweep of standard FTO glass by Vander pauw method

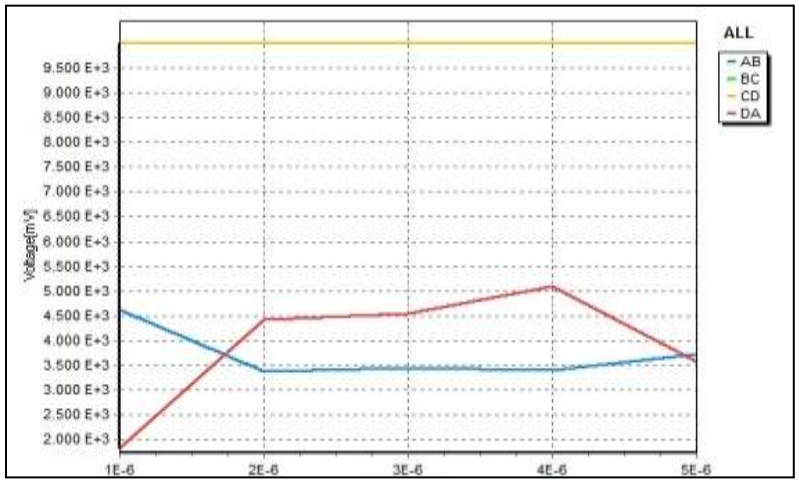

Fig.12 (b) Current-Voltage sweep of ZnS thin film on FTO glass by vander pauw method

The electrical properties such as resistivity, conductivity, mobility, hall coefficient, and carrier concentration of deposited films are directly estimated by the Hall Effect measuring system by the Vander Pauw method [28]. **Figure 11** shows the four-probe Vander Pauw method.

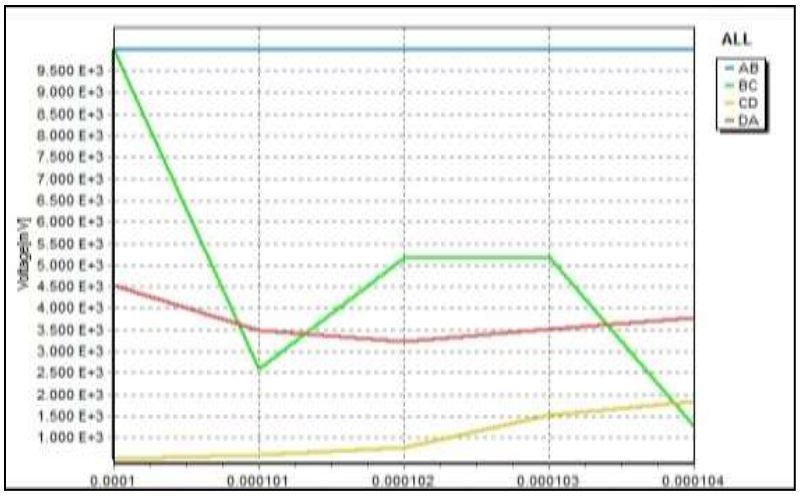

Fig.12 (c) Current-Voltage sweep of ZnS: Cu (1%) thin film on FTO glass by vander pauw method

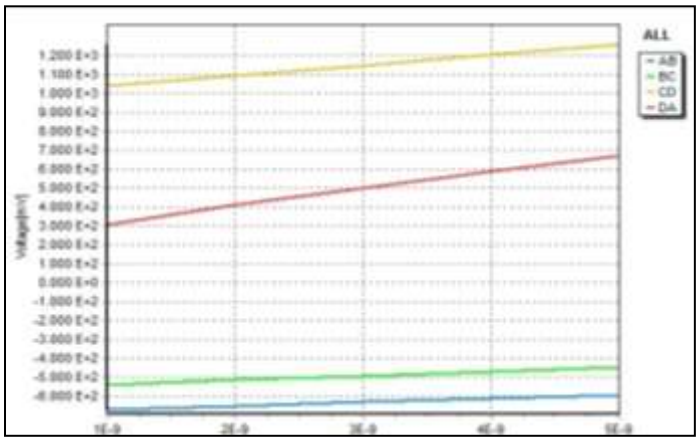

Fig.12 (d) Current-Voltage sweep of ZnS: Cu (2%) thin film on FTO glass by vander pauw method

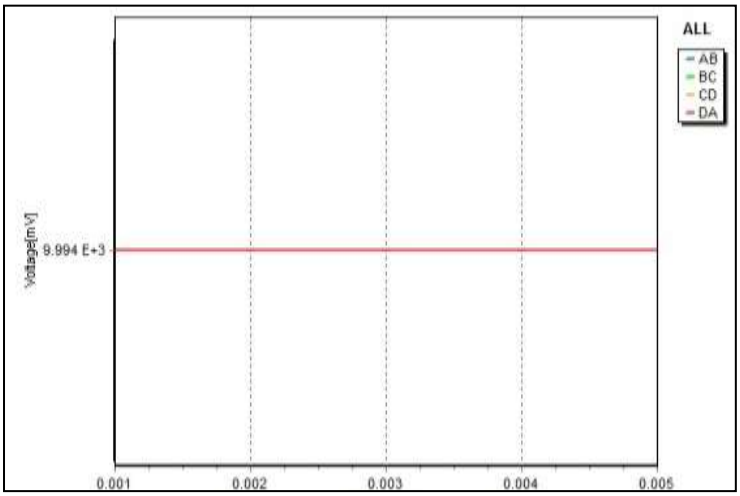

Fig.12(e) Current-Voltage sweep of ZnS: Cu (3%) thin film on FTO glass by vander pauw method

From **Figure 12** (a), (b), (c), (d), and (e) the resistivity of Pure ZnS, ZnS: Cu(1%), ZnS: Cu(2%), and ZnS: Cu(3%) film samples were observed about 1.782 x 10^6 **Ω**/cm, 1.081x10^6 **Ω**/cm, 2.789x10^4 **Ω**/cm and 2.235x10^3 **Ω**/cm respectively. The resistivity of films reduced in the range of 10^6 -10^3 **Ω**/cm with enhancing Cu-doping in ZnS thin film [29]. This is due to the concentration of electrons increases. The Cu ions can be incorporated on Zn sites acts as acceptor impurity and on interstitial sites acts as a donor impurity. Here is confirmed the Cu ions incorporated on interstitial sites. So the concentration of electrons increases. The carrier concentration of films Undoped ZnS and ZnS: Cu (1%), ZnS: Cu (2%) and ZnS: Cu (3%) were estimated about -1.7815x10^{11} /cm^3, -2.5867x10^{11} /cm^3, -1.6412x10^{12} /cm^3 and -2.9519x10^{12}/cm^3 respectively. The carrier concentration was observed highest value at Cu (3%) in ZnS due to ZnS play donor type impurity. The mobility of Pure ZnS and ZnS: Cu (1%), ZnS: Cu (2%) and ZnS: Cu (3%) were observed about 0.1234x10^2 cm^2/vs, 2.6843x10^2 cm^2/vs, 6.2178x10^3 cm^2/vs and 9.4612x10^3 cm^2/vs respectively. The mobility was also found highest at Cu (3%) in ZnS due to low resistivity and high electron concentration. The average hall coefficient of deposited thin film samples was found -2.0785x$10^6$$cm^3$/c. It is confirmed the negative value indicates the film exhibit n-type electrical conductivity. The electrical and optical parameters are listed in Table.5

Table.5: Electro-optical properties of Un and Cu-doped ZnS thin films

Electro-Optical Properties	Undoped ZnS	ZnS: Cu (1%)	ZnS: Cu (2%)	ZnS: Cu (3%)
Resistivity(Ω/cm)	1.782x10^6	1.081x10^6	2.789x10^4	2.235x10^3
Carrier concentration(/cm^3)	-1.781x10^{11}	-7.586x10^{11}	-1.641x10^{12}	-2.951x10^{13}
Mobility(cm^2/vs)	0.1234x10^2	2.6843x10^2	6.2178x10^3	9.4612x10^3
Hall coefficient(cm^3/c)	-1.5362x10^6	-1.6812x10^6	-2.1146x10^6	-2.9821x10^6
Energy band gap(eV)	3.97	3.07	2.45	2.11

4. Conclusion:

The Pure and Cu-doped ZnS thin film successfully deposited on stainless steel and FTO substrates by simplified 2-electrode electrodeposition method. The electrochemical behavior of Zn, S, and Cu was investigated by the cyclic voltammetry technique for good deposition carried out by the 2-electrode method. The XRD pattern of doped film samples have seen a Zincblende cubic structure. The lattice constant of ZnS thin films decreases in the range 5.452- 5.424 A^0 by increasing Cu-doping in ZnS due to lattice microstrain and Cu ions incorporated in the interstitial site of Zn. The crystallite size of ZnS thin films decreases with increasing copper (range 34.46- 18.02 nm). Also peak intensity of ZnS thin films have been seen reduced. The XRD pattern of 3% Copper doped ZnS film showed maximum value of dislocation density and microstrain of films. SEM micrograph showed the hexagonal grain morphology in 3% copper doped ZnS film sample. The energy band gap was decreased by enhancing Copper in ZnS thin film. 2% copper doped ZnS film sample showed the highest transparency due to a low refractive index up to wavelength 718 nm. They can be used as a window layer or buffer layer in the modified solar cell. The electrical resistivity of copper doped ZnS film samples varied in the range 1.782 x 10^6 to 2.235x$10^3\Omega$/cm. The highest carrier concentration and mobility were found at about -2.951x10^{13}/cm^3, 9.4612 x $10^3$$cm^2$/Vs respectively in samples of 3% copper doped ZnS. The average value of hall coefficient of all deposited films was found to -2.0785 x $10^6$$cm^3$/c. From this, 2% copper doped ZnS thin film sample may be used as a window or buffer layer in a thin-film heterojunction solar cell device.

Acknowledgment:
The authors are thankful to the Research Center in Physics, Mahatma Gandhi Vidyamandir's Panchavati Nashik for conducting research work. Also thankful to SAIF- IIT Bombay, SAIF-IIT Kanpur, and CIF Chandigarh University Punjab for sample characterization.

Compliance with ethical standards:
Conflict of interest Authors declares no conflict of interest.

References:
[1] Alireza Goudarzi, Ghaffar Motedayen Aval, Reza Sahraei, Hiva Ahmadpoor, Ammonia-free chemical bath deposition of nanocrystalline ZnS thin film buffer layer for solar cells, Thin Solid Films. 2008, 516, P-4953-4957. https://doi.org/10.1016/j.tsf.2007.09.051
[2] Naglaa Fathy, Masaya Ichimura, Photoelectrical properties of ZnS thin films deposited from aqueous solution using pulsed electrochemical deposition, Solar Energy Materials and Solar Cells, 2005,87, P-747-756. https://doi.org/10.1016/j.solmat.2004.07.048
[3] H.M.M.N. Hennayaka, Ho Seong Lee, Structural and optical properties of ZnS thin film grown by pulsed electrodeposition, Thin Solid Films, 2013, 548, P-86-90. https://doi.org/10.1016/j.tsf.2013.09.011
[4] Poulomi Roy, Jyoti R.Ota, Suneel Kumar Srivastava, Crystalline ZnS thin films by chemical bath deposition method and its characterization, Thin Solid Films, 2006, 515, P- 1912-1917. https://doi.org/10.1016/j.tsf.2006.07.035
[5] J.Wang,T.Li, Q.Wang,W.Wang, R.Shi, N.Wang, A.Amini, C.Cheng, Controlled growth of atomically thin transition metal dichalcogenides via chemical vapor deposition method, Material todays advances, 2020, 8, P-100098. https://doi.org/10.1016/j.mtadv.2020.100098
[6] J.M.Blackmore, A.G.Cullis, The structure of ZnS thin films deposited by r.f. sputtering, Thin Solid Films, 1991, 199, P-321-334 https://doi.org/10.1016/0040-6090(91)90014-O
[7] EdwinJose, M.C.Santhosh Kumar, Room temperature deposition of highly crystalline Cu-Zn-S thin films for solar cell applications using SILAR method, Journal of Alloys and Compounds, 2017, 712, P-649-656. https://doi.org/10.1016/j.jallcom.2017.04.097
[8] Tayfur Kucukomeroglu, Emin Bacaksiz, CabirTerzioglu, AhmetVarilci, Influence of fluorine doping on structural, electrical and optical properties of spray pyrolysis ZnS films, Thin Solid Films, 2008,516, P-2913-2916 https://doi.org/10.1016/j.tsf.2007.05.075
[9] G Contreras-Puente, OVigil, MOrtega-López, AMorales-Acevedo, JVidal, M.LAlbor-Aguilera, New window materials used as heterojunction partners on CdTe solar cells, Thin Solid Films, 2000, 361–362, P- 378-382. https://doi.org/10.1016/S0040-6090(99)00806-8
[10]Hyun JooLee, Soo IlLee, Deposition and optical properties of nanocrystalline ZnS thin films by a chemical method, Current Applied Physics, 2007, 7, P-193-197. https://doi.org/10.1016/j.cap.2006.03.005
[11] S.KMandal, SChaudhuri, A.K Pal, Optical properties of nanocrystalline ZnS films prepared by high pressure magnetron sputtering, Thin Solid Films, 1999, 350, P-209-213 https://doi.org/10.1016/S0040-6090(99)00236-9
[12] Z.Z.Zhang, D.Z.Shen, J.Y.Zhang, C.X.Shan, Y.M.Lu, Y.C.Liu, B.H.Li, D.X.Zhao, B.Yao, X.W.Fan, The growth of single cubic phase ZnS thin films on silica glass by plasma-assisted metalorganic chemical vapor deposition, Thin Solid Films. 2006, 513, P-114-117. https://doi.org/10.1016/j.tsf.2006.01.054
[13] Sema Ebrahimi, Benyamin Yarmand, Nima Naderi, Enhanced Optoelectrical properties of Mn-doped ZnS films deposited by spray pyrolysis for ultraviolet detection applications, Thin Solid Films. 2019, 676, P-31-41. https://doi.org/10.1016/j.tsf.2019.02.046

[14] T.Vdovenkova, A.Vdovenkov, R.Tornqvist, ZnS wide band gap semiconductor thin film electronic structure sensitivity to Mn impurity, Thin Solid Films.1999,343–344, P-332-334. https://doi.org/10.1016/S0040-6090(98)01596-X
[15] M.A.Hernández-Fenollosa, M.C.López, V.Donderis, M.González, B.Marí, J.R.Ramos-Barrado, Role of precursors on morphology and optical properties of ZnS thin films prepared by chemical spray pyrolysis, Thin Solid Films. 2008, 516, P-1622-1625. https://doi.org/10.1016/j.tsf.2007.05.031
[16]JunLiuAixiangWei, YuZhao, Effect of different complexing agents on the properties of chemical-bath-deposited ZnS thin films, Journal of Alloys and Compounds. 2014, 588, P- 228-234. https://doi.org/10.1016/j.jallcom.2013.11.042
[17] M.Shobana, S.R.Meher, Effect of cobalt doping on the structural, optical and magnetic properties of sol-gel derived ZnS nanocrystalline thin films and ab initio studies, Thin solid films. 2019, 683, P- 97-110. https://doi.org/10.1016/j.tsf.2019.05.037
[18] X.D.Gao, X.M.Li, W.D.Yu, Morphology and optical properties of amorphous ZnS films deposited by ultrasonic-assisted successive ionic layer adsorption and reaction method, Thin Solid Films. 2004, 468, P-43-47. https://doi.org/10.1016/j.tsf.2004.04.005
[19] Evren Turan, Muhsin Zor, A. Senol Aybek, Metin Kul, Electrical properties of ZnO/Au/ZnS/Au films deposited by ultrasonic spray pyrolysis, Thin Solid Films. 2007, 515, P- 8752-8755. https://doi.org/10.1016/j.tsf.2007.04.001
[20] Taisuke Iwashita, Shizutoshi Ando, Preparation and characterization of ZnS thin films by the chemical bath deposition method, Thin Solid Films. 2012, 520, P-7076-7082 https://doi.org/10.1016/j.tsf.2012.07.129
[21] T.Kryshtab, V.S.Khomchenko, J.A.Andraca-Adame, L.V.Zavyalova, N.N.Roshchina, V.E.Rodionov, V.B.Khachatryan, Preparation and properties of thin ZnS:Cu films phosphors, Thin Solid Films.2006, 515, P-513-516. https://doi.org/10.1016/j.tsf.2005.12.284
[22] V.S.Ganesha Krishna, M.G.Mahesha, Characterization of transparent p-type Cu:ZnS thin films grown by spray pyrolysis technique, Journal of Alloys and Compounds.2020, 848, P- 156568. https://doi.org/10.1016/j.jallcom.2020.156568
[23] M.E Rincón, M.W Martínez, M Miranda-Hernández, Nano structured vs. polycrystalline CdS/ZnS thin films for photocatalytic applications ,Thin Solid Films. 2003, 425, P-127-134. https://doi.org/10.1016/S0040-6090(02)01301-9
[24] H.H.Afifi , S.A.Mahmoud, A.A shour, Structural study of ZnS thin films prepared by spray pyrolysis, Thin Solid Films. 1995, 263, P-248-251. https://doi.org/10.1016/0040-6090(95)06565-2
[25] G.Leftheriotis, P.Yianoulis, D.Patrikios, Deposition and optical properties of optimized ZnS/Ag/ZnS thin films for energy saving applications, Thin Solid Films. 1997, 306, P-92-99. https://doi.org/10.1016/S0040-6090(97)00250-2
[26]J.Díaz-Reyes, R.S.Castillo-Ojeda, R.Sánchez-Espíndola, M.Galván-Arellano, O.Zaca-Morán, Structural and optical characterization of wurtzite type ZnS, Current Applied Physics. (2015),15, P-103-109. https://doi.org/10.1016/j.cap.2014.11.012
[27] Mingyue Sun,JunchengLiu, BeipingDong, Effects of Sb doping on the structure and properties of SnO_2 films, Current Applied Physics. 2020, 20, P-462-469. https://doi.org/10.1016/j.cap.2020.01.009
[28] K.Nagamani,N.Revathi, P.Prathap, Y.Lingappa, K.T. Ramakrishna Reddy, Al-doped ZnS layers synthesized by solution growth method, Current Applied Physics. 2012, 12, P-380-384. https://doi.org/10.1016/j.cap.2011.07.031
[29] John L.Davis Bland B.Houston, Antonio Martinez, Preparation and properties of epitaxial films of indium-doped lead tin telluride, Thin Solid Films. 1984, 122, P-217-229. https://doi.org/10.1016/0040-6090(84)90049-X